Available online at www.sciencedirect.com
ScienceDirect
International Journal of Heat and Mass Transfer 51 (2008) 4875–4885
International Journal of HEAT and MASS TRANSFER
www.elsevier.com/locate/ijhmt

# Semi-analytical solution of the extended Graetz problem for combined electroosmotically and pressure-driven microchannel flows with step-change in wall temperature

Arun Sharma, Suman Chakraborty *

*Department of Mechanical Engineering, Indian Institute of Technology, Kharagpur 721302, India*

Received 6 June 2007; received in revised form 29 January 2008
Available online 28 April 2008

**Abstract**

Analytical solutions are obtained for the temperature and Nusselt number distribution in the thermal entrance region of a parallel plate microchannel under the combined action of pressure-driven and electroosmotic transport mechanisms, by taking into account the effects of viscous dissipation, Joule heating and axial conduction simultaneously, in the framework of an extended Graetz problem. Step changes in wall temperature are considered to represent physically conceivable thermal entrance conditions. The solution of the temperature distributions at the various channel sections essentially involves the determination of a set of eigenvalues and eigenfunctions corresponding to a Sturm Liouiville problem with non self-adjoint operators. The resultant eigenfunctions are non orthogonal in nature, and are obtained in the forms of hypergeometric functions. Parametric variations on the effects of the relative strengths of the pressure gradients and the electric field, ratio of the rate of heat generation to the rate of wall heat transfer, and the Peclet number are analyzed in details, in terms of their influences on the temperature field as well as the Nusselt number distribution.


## 1. Introduction

With challenging demands for high throughput screening in biomedical and biotechnological applications, micro-scale transport processes have been receiving increasingly intensive attention from the concerned research community over the past few years. Various flow actuation methodologies have been explored by the researchers for efficient design of such microfluidic systems. In many practical applications involving the Lab-on-a-Chip based Micro-Total-Analysis systems, electroosmotic flow actuation mechanisms [1–4] have been found to offer with extremely efficient methodologies for manipulating the transport of polar solvents (often carrying different types of biological samples). Fundamentally, the origin of electroosmotic flows through microchannels can be attributed to the fact that when a solid is in contact with an electrolyte, the chemical state of the surface is generally altered, either by ionization of covalently bound surface groups or by ion adsorption. As a result, the surface inherits a charge while counter-ions are released into the liquid. At equilibrium, a balance between electrostatic interactions and thermal agitation generates a charge density profile. The liquid is electrically neutral, but for a charged layer adjacent to the boundary, which bears a charge locally equal in amplitude and opposite in sign to the bound charge on the surface. This charged layer is commonly known as the electric double layer (EDL). If a potential gradient is applied along the microchannel axis in presence of the charge density distribution within the EDL, fluid elements located within the diffuse EDL tend to move under the action of electrostatic forces. Due to a cohesive nature of the hydrogen bonding in the polar solvent molecules, the entire buffer solution is pulled, leading to a net electrokinetic body force on the bulk fluid. This electroosmotic force, in effect, is a combined function of the charge density distribution and the imposed electric field.

* Corresponding author.
*E-mail address:* suman@mech.iitkgp.ernet.in (S. Chakraborty).

0017-9310/$ - see front matter © 2008 Elsevier Ltd. All rights reserved.
doi:10.1016/j.ijheatmasstransfer.2008.02.041

**Nomenclature**

| | |
|---|---|
| $a$ | channel half width [m] |
| $A_n$, $B_n$ | expansion coefficients |
| $E_x$ | electric field in stream wise direction [V/m] |
| $f_n$, $g_n$ | eigenfunctions |
| $G_1$ | normalized generation term $E_x^2\sigma a^2/k(T_0 - T_w)$ |
| $G_2$ | normalized viscous dissipation term $\mu U_{HS}^2/k(T_0 - T_w)$ |
| $Pe$ | Peclet number |
| $T_o$ | wall temperature in upstream region [K] |
| $T_w$ | wall temperature in downstream region [K] |
| $Nu$ | Nusselt number |
| $Nu_i$ | local Nusselt number |
| $u(\eta)$ | dimensionless velocity profile |
| $U_{HS}$ | Helmholtz–Smoluchowski velocity [m/s] |
| $x$ | axial coordinate [m] |
| $y$ | transverse coordinate [m] |
| $k_B$ | Boltzmann constant ($1.3805 \times 10^{-23}$ J mol$^{-1}$ K$^{-1}$) |
| $\eta$ | dimensionless transverse coordinate $y/a$ |
| $\theta$ | dimensionless temperature distribution $T - T_w/T_0 - T_w$ |
| $\theta_b$ | dimensionless bulk mean temperature |
| $\theta_p$ | particular solution to dimensionless temperature distribution |
| $\Omega$ | normalized pressure gradient |
| $\xi$ | dimensionless axial coordinate $x/aPe$ |
| $\sigma$ | electrical conductivity [S/m] |
| $\psi$ | electro kinetic potential [V] |
| $\rho$ | fluid density [kg/m$^3$] |
| $\rho_e$ | electric charge density [C/m$^3$] |
| $\varepsilon$ | fluid dielectric constant |
| $\varepsilon_0$ | permittivity of vacuum ($8.85 \times 10^{-12}$ C V$^{-1}$ m$^{-1}$) |
| $\zeta$ | zeta potential [V] |
| $\alpha$ | thermal diffusivity [m$^2$/s] |
| $\mu$ | dynamic viscosity [N s/m$^2$] |

*Greek symbols*

| | |
|---|---|
| $\lambda_n$, $\beta_n$ | eigenvalues |

As compared to the conventional pressure-driven flow mechanisms, the electroosmotic flow offers with several advantages, such as much simpler operations in the absence of any moving components and plug-like velocity profiles characterized with less severe solute dispersion effects. However, despite having these advantageous features, electroosmotic flow mechanisms are also associated with inevitable side effects of Joule heating. This internal heat generation might give rise to uncontrolled rises in temperature, which might be detrimental for the handling of thermally labile biological samples. Research studies [2,3] have already demonstrated that the effects of Joule heating can result in low column separation efficiency, reduction of analysis resolution, and even loss of injected samples. Additionally, temperature rise in microchannels due to Joule heating has been found to be responsible for the unwarranted formation of gas bubbles. Moreover, for handling biological macromolecules (such as DNA) with high negative electrophoretic mobilities, electroosmotic pumping of the sample necessitates a buffer with a large electroosmotic mobility so that the driving electroosmotic forces can overcome the negative electrophoretic mobility of the macromolecules. Unfortunately, buffers used in macromolecular separation or hybridization often contain salts in high concentrations, which reduce the electroosmotic effects to a considerable extent. In that perspective, pumping using mechanical pressure might possess some advantages over the electroosmotic approach in the sense that the former is insensitive to the variations in pH, macromolecular charges and the salt concentration. However, because of the huge pumping power requirements and considerable sample dispersion, mechanical pumping alone might not be a preferred mechanism for driving fluid flow through micro-scale conduits for these applications. Furthermore, because of the high back-pressures generated due to the considerable flow resistances associated with mechanically-pumped microchannel flows involving large pressure gradients, leakage prevention might itself pose a challenging operational problem, if the unit is not properly sealed. As a compromise, researchers have recently proposed [2] the employment of combined electroosmotic and pressure-driven transport mechanisms for pumping the flow of liquids through microchannels, especially for biotechnological applications.

Although several theoretical studies have appeared in the literature describing the hydrodynamics of electroosmotic flow through circular and rectangular microchannels, relatively little prior work has appeared in the literature on the characterization of convective heat transfer associated with electroosmotic flows. Recently, Maynes and Webb [5] presented a detailed thermal analysis of electroosmotic flows in circular microtubes and parallel plate microchannels. Extending these underlying principles, Chakraborty [6] developed closed form expressions for Nusselt number variations in thermally fully developed microtube flows, under the combined influence of electroosmotic forces and imposed pressure gradients. However, the above-mentioned studies were limited only towards analyzing the thermally fully developed transport regimes. Horiuchi and Dutta [7], for the first time, obtained semi-analytical solutions for temperature distributions and heat transfer characteristics in the thermally developing regimes

of electroosmotic flows in microchannels. Their analysis accounted for the interaction between convection, viscous, and Joule heating terms, so as to obtain the temperature distribution in the microchannel. This analysis was based on an infinitesimal electric double layer thickness, in which the velocity profiles are virtually of 'plug' type, except for a very thin layer (essentially the EDL) very close to the wall. Both the constant surface temperature and the constant surface heat flux conditions were considered in their study. The method of separation of variables was employed to obtain expressions for temperature distributions from the energy conservation equation for electroosmotically driven flows. Heat transfer characteristics were presented for low Reynolds number microflows, in which the viscous and Joule heating effects are likely to be of profound importance. For the parameter range covered in their study, the Nusselt number was found to be independent of the thermal Peclet number, except in the thermally developing region. Results for the cases with and without Joule heating were also compared successfully in their study.

From an extensive review of the published literature, it is revealed that there have been only few attempts reported in the literature to solve the Graetz problem defined on an appropriate physical basis of electroosmotically driven microchannel flows. The original Graetz problem, as discussed in the literature more than a century ago, is a simplified problem of laminar forced convective heat transfer in a circular tube, which was first analytically solved by Graetz [8], by assuming hydrodynamically fully developed flow and neglecting streamwise heat conduction and viscous dissipation. Sellars et al. [9] extended the original Graetz problem, including a more effective approximation technique for solving the eigenvalues problem. Lahjomri et al. [10] extended the solution of the Gratez problem to include streamwise conduction effects. Several researchers [11,12] in the recent past presented analytical solutions of the Gratez problem for microchannel gas flows, incorporating wall-slip boundary conditions. Dutta et al. [13], in a very recent study, numerically analyzed the thermally developing characteristics of mixed electroosmotic and pressure-driven microflows. This study was executed with the classical consideration of a prescribed uniform temperature profile at the channel inlet. Although this consideration is consistent with the definition of a well-posed mathematical problem, the practical aspects of the same may be seriously questioned. This is because of the fact that in practice, it is virtually an impossible proposition to maintain the thermal entrance temperature to be uniform, in presence of heat sources such as viscous dissipation and Joule heating. In fact, with an arbitrarily imposed uniform temperature profile at the channel inlet, it is hard to conceptualize an experimental procedure without disturbing the hydrodynamically fully developed velocity field that is consistent with the solution of the Graetz problem [14]. However, no study has yet been reported in the literature to offer with a detailed analysis of the thermal entrance region for electrokinetically driven microchannel flows by incorporating such considerations of physically conceivable thermal entrance conditions, in the form of an extended Graetz problem.

Aim of the present study is to obtain analytical solutions for the extended Gratez problem in combined electroosmotically and pressure driven microchannel flows, with a simultaneous consideration of the effects of streamwise conduction, viscous dissipation, and Joule heating, corresponding to a step-change in wall temperature that physically mimics the thermal condition at the channel entrance. The effect of axial heat conduction becomes important at low Peclet numbers. The problem is considered in two semi infinite regions of the channel, in upstream $(-\infty < x < 0)$ and downstream $(0 < x < \infty)$ regions.The temperature is then determined in both regions and the two solutions are matched at $x = 0$ where the heating or cooling starts. This type of problem is related to determination of a set of eigenvalues and eigenfunctions of Sturm Liouiville non self-adjoint operators. The result is that the eigenfunctions become non orthogonal and simple determination of related expansion coefficients by classical method fails. Because of the presence of axial heat conduction term, transverse variations in temperature exists in region $x < 0$ because of the heat conducted upstream. The main difficulty comes from the singularity which exists for channel wall temperature for $x = 0$, which creates a problem for numerical modelers. Therefore, analytical solution is required to resolve the singularity. In effect, temperature distributions in the channel are determined as parametric functions of the relative strengths of the pressure-driven and electroosmotic flow components, and the relative strengths of Joule heating and viscous dissipation with respect to the thermal conduction effects. Several limiting cases are also retrieved from the analytical solution, corresponding to the thermally fully developed condition.

## 2. Mathematical modeling

We consider a combined electroosmotically and pressure-driven fluidic transport through a long parallel plate microchannel of height $2a$, and width $W$, with $W \gg 2a$.

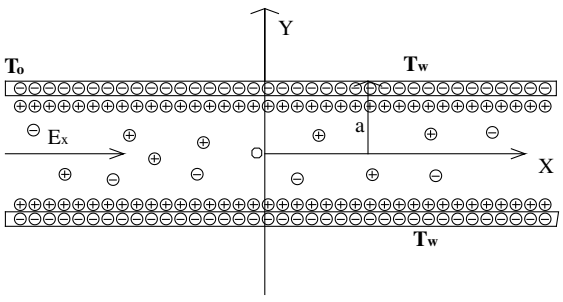


Fig. 1. A schematic representation of the physical problem, where the step jump in wall temperature at $X = 0$ mimics the thermal entrance condition.

The fluid flow is acted upon by an axial electric field of strength $E_x$, as shown in Fig. 1. Over and above this electric field, a constant axial pressure gradient $P_x = -\frac{dp}{dx}$ acts on the fluid. The flow is assumed to be hydrodynamically fully developed. The channel walls are maintained at temperature $T_0$ for $x < 0$. The wall temperature is suddenly changed to $T_w$ for $x > 0$. For the present mathematical analysis, following major assumptions are made:

(i) The fluid is Newtonian and incompressible.
(ii) The fluid viscosity is independent of the local ionic concentration.
(iii) Fluid properties are not appreciably sensitive to the changes in temperature, over the temperature range considered in this study (~10 K).
(iv) The solvent is continuous, and its permittivity is unaffected by the electric field strength.
(v) The ionic species behave as point charges.
(vi) The zeta potential is uniform throughout the channel walls.
(vii) The Boltzmann distribution of ionic concentration remains valid. This assumption is justified when there is negligible axial gradient of the ionic concentration within the microchannel and the flow Peclet number is sufficiently small, which are considered to be appropriate for the present study. Another important assumption that goes with this consideration is that the EDLs formed in vicinity of the microchannel walls do not overlap and protrude into the centerline, so that a far-stream boundary condition for the ionic charge densities can be imposed on the channel centerline.
(viii) The volumetric heating arises from the conduction current only and may be safely modeled using Ohm's law. Further, this energy generation is assumed to be distributed uniformly across the channel cross-section, which is a justified proposition for low zeta potential or for large hydraulic diameter-to-Debye length ratios, as considered in the present study.

The fundamental origin of the EDL effects lies in the fact that the channel walls may attain a net positive or negative charge due to ion adsorption from the polar liquid molecules adjacent to the solid surface. This surface charge is effectively balanced by the counter-ions present in the fluid medium. There is a thin layer of ions adsorbed on the charged surface, which is known as the Stern layer. The outer region, where ions are in rapid thermal motion, is called the diffuse EDL. The EDL formed is typically of the order of a few nm in thickness or somewhat thicker, depending on ionic concentration of the solution (higher the ion concentration, lower the EDL thickness). When the EDL thickness is much smaller than the channel hydraulic radius, the probability of finding an ion at a particular point within the EDL is proportional to the Boltzmann factor, $e^{-ze\psi/k_BT}$, where $z$ is the valence of the concerned charge, $e$ is the electronic charge, $\psi$ is the electroosmotic potential, $k_B$ is the Boltzmann constant and $T$ is absolute temperature. Accordingly, for a binary fluid consisting of two kinds of ions of equal and opposite charge $z^+$ and $z^-$, the number of ions of each type can be described by the Boltzmann distribution, given as: $n^- = n_0 e^{ze\psi/k_BT}$ and $n^+ = n_0 e^{-ze\psi/k_BT}$, where $n_0$ is the average number of positive or negative ions in the buffer. The net charge density per unit volume is accordingly given as

$$\rho = (n^+ - n^-)ze = -2n_0 ze \sinh(ze\psi/k_BT) \tag{1}$$

Based on this charge density distribution, the electroosmotic potential distribution can be readily obtained by employing the Poisson–Boltzmann equation, which is of the form [7]:

$$\nabla^2\psi = -\frac{\rho}{\varepsilon\varepsilon_0} \tag{2}$$

where $\varepsilon$ is the dielectric constant of the medium and $\varepsilon_0$ is permittivity of vacuum. In the present case, the above leads to the following ordinary differential equation:

$$\frac{d^2\psi}{dy^2} = \frac{2n_0 ze}{\varepsilon\varepsilon_0}\sinh\left(\frac{ze\psi}{k_BT}\right) \tag{2a}$$

The variables appearing in the above equations can be non-dimensionalized by employing suitable non-dimensional parameters as: $\eta = \frac{y}{a}$, $\bar{\psi} = \frac{ze\psi}{k_BT}$ and $\bar{\rho}(\eta) = \frac{\rho(\eta)}{n_0 ze}$, so as to obtain

$$\frac{d^2\bar{\psi}}{d\eta^2} = k^2\sinh(\bar{\psi}) \tag{3}$$

where $k = (a/\lambda_D)$, with $1/\lambda_D = (2n_0 z^2 e^2/\varepsilon\varepsilon_0 k_B T)^{-\frac{1}{2}}$. Here, $\lambda_D$ is the characteristic thickness of the EDL, also known as the Debye length. We further assume here that the wall zeta potential is small enough ($\zeta < 3k_BT$) so that the Debye–Hückel linearization approximation can be applied [11]. With the pertinent boundary conditions as $\bar{\psi} = \bar{\zeta}$ at $\eta = \pm 1$ (where $\bar{\zeta} = \frac{ze\zeta}{k_BT}$), or equivalently, $\frac{d\bar{\psi}}{d\eta} = 0, \eta = 0$, the linearized Poisson Boltzmann equation can be solved, to obtain the EDL potential distribution as

$$\bar{\psi} = \frac{\bar{\zeta}}{\cosh(k)}\cosh(k\eta) \tag{4}$$

Using this potential variation, one may obtain the following charge density distribution:

$$\rho(\eta) = n_0 ze\bar{\rho}(\eta) = -2n_0 ze\sinh(\bar{\psi}) \approx -2n_0 ze\bar{\psi} = -\frac{k^2\varepsilon\zeta}{a^2}\frac{\cosh(k\eta)}{\cosh(k)} \tag{4a}$$

In presence of the above-mentioned charge density distribution, if a potential gradient is applied along the channel axis, fluid elements located within the diffuse EDL tend to move under the action of electrostatic forces. Due to a cohesive nature of the hydrogen bonding in the polar solvent molecules, the entire buffer solution is pulled, leading to a net electrokinetic body force on the bulk fluid. This electroosmotic force is a combined function of the charge

density distribution and the imposed electric field. Superimposed on this effect is the influence of an applied pressure gradient, which gives rise to the steady state velocity distribution within the microchannel. This can be obtained by solving the Navier–Stokes equation, described as

$$\rho_f(\vec{u}\cdot\vec{\nabla})\vec{u} = -\vec{\nabla}p + \mu\nabla^2\vec{u} + \vec{F} \tag{5}$$

where $\vec{u}$ is the velocity field, $\rho_f$ is the fluid density, $p$ is the pressure, $\mu$ is the dynamic viscosity. For a hydrodynamically fully developed flow, Eq. (5) gets simplified to the following form:

$$-\frac{dp}{dx} + \mu\frac{d^2u}{dy^2} + \rho E_x = 0 \tag{6}$$

Subjected to the boundary conditions: $u(y=a)=0$, $\frac{du}{dy}(y=0)=0$, Eq. (6) can be analytically solved, to obtain the following velocity profile in a non-dimensional form:

$$\frac{u}{U_{HS}} = \frac{-P_x a^2}{2\mu U_{HS}}(1-\eta^2) + \left(1 - \frac{\cosh(k\eta)}{\cosh k}\right) \tag{7}$$

where $U_{HS} = \frac{-\varepsilon\zeta E_x}{\mu}$ is a reference electroosmotic velocity. It is also important to note here that while interpreting the above solution, one may mathematically approximate the electroosmotic flow from an equivalent slip velocity consideration, which allows one to neglect the details of the charge distribution within the double layer, based on the consideration that $\left(1 - \frac{\cosh(k\eta)}{\cosh k}\right) \approx 1$ for almost over the entire channel cross-section, except for within the thin EDL. This assumption has been successfully employed by many researchers, including the studies recently reported by Horiuchi and Dutta [7], with an understanding that the contribution of the electrososmotic fields towards the viscous dissipation effects may be taken as negligible as compared to the corresponding influences on the Joule heating effects, provided that the channel hydraulic radius is at least one order of magnitude larger than the characteristic EDL thickness. Considerations adopted in the present study, indeed, support this conjecture, so that one may write: $u(\eta) = \frac{u}{U_{HS}} = \Omega(1-\eta^2) + 1$, where $\Omega = \frac{\frac{-P_x a^2}{2\mu}}{U_{HS}}$.

For obtaining the temperature distribution, the energy equation can be employed in the following form:

$$\rho_f c_p u\frac{\partial T}{\partial x} = k\left(\frac{\partial^2 T}{\partial x^2} + \frac{\partial^2 T}{\partial y^2}\right) + \mu\left(\frac{\partial u}{\partial y}\right)^2 + E_x^2\sigma \tag{8}$$

where $k$ is thermal conductivity, $c_p$ is the specific heat, $i$ is the ionic current density, and $\sigma$ is the electrical conductivity. The penultimate term in the right hand side of Eq. (8) represents the effects of viscous dissipation, and the final term represents the effects of Joule heating. Introducing the following normalization parameters: $\theta = \frac{T-T_w}{T_0-T_w}$, $\xi = \frac{x}{aPe}$, $Pe = \frac{U_{HS}a}{\alpha}$, $\alpha = \frac{k}{\rho C_p}$, $G_1 = \frac{E_x^2\sigma a^2}{k(T_0-T_w)}$, $G_2 = \frac{\mu U_{HS}^2}{k(T_0-T_w)}$, Eq. (8) can be expressed in a non dimensional form, as

$$u(\eta)\frac{\partial\theta}{\partial\xi} = \frac{1}{Pe^2}\left(\frac{\partial^2\theta}{\partial\xi^2}\right) + \frac{\partial^2\theta}{\partial\eta^2} + G_2\left(\frac{\partial u}{\partial\eta}\right)^2 + G_1 \tag{9}$$

so that

$$\theta = \theta_1 \quad \text{for } -\infty < \xi < 0 \tag{9a}$$

$$\theta = \theta_2 \quad \text{for } 0 < \xi < \infty \tag{9b}$$

The pertinent boundary conditions are as follows:

$$\frac{\partial\theta_i}{\partial\eta} = 0 \quad \text{for } \eta = 0\ \forall -\infty < \xi < \infty\ (i=1,2) \tag{10a}$$

$$\theta_1 = 1 \quad \text{for } \eta = 1\ \forall -\infty < \xi < 0 \tag{10b}$$

$$\theta_2 = 0 \quad \text{for } \eta = 1\ \forall 0 < \xi < \infty \tag{10c}$$

$$\theta_1 = 1 \quad \text{for } \xi \to -\infty\ \forall 0 \leqslant \eta \leqslant 1 \tag{10d}$$

$$\theta_2 = 0, \quad \text{for } \xi \to +\infty\ \forall 0 \leqslant \eta \leqslant 1 \tag{10e}$$

$$\theta_1 = \theta_2 \quad \text{for } \xi = 0\ \forall 0 \leqslant \eta \leqslant 1 \tag{10f}$$

$$\frac{\partial\theta_1}{\partial\xi} = \frac{\partial\theta_2}{\partial\xi} \quad \text{for } \xi = 0\ \forall 0 \leqslant \eta \leqslant 1 \tag{10g}$$

For very large values of $\xi$ (i.e., $\xi \to \pm\infty$), the temperature profile is represented by particular integral of the following equation:

$$\frac{\partial^2\theta}{\partial\eta^2} + G_2\left(\frac{\partial u}{\partial\eta}\right)^2 + G_1 = 0 \tag{11}$$

The above equation satisfies the following boundary conditions:

$$\left(\frac{\partial\theta}{\partial\eta}\right)_{\eta=0} = 0 \tag{12a}$$

$$\theta_{\eta=1} = 0 \ \text{ for } \xi\to\infty \ \text{ and } \ \theta_{\eta=1} = 1 \ \text{ for } \xi\to-\infty \tag{12b}$$

The general solution of Eq. (9) in the upstream and downstream region, satisfying the above boundary conditions, can be represented as follows:

$$\theta_1 = 1 + \sum_{n=1}^{\infty} A_n f_n(\eta) e^{\lambda_n^2\xi} + \theta_p \tag{13a}$$

$$\theta_2 = \sum_{n=1}^{\infty} B_n g_n(\eta) e^{-\beta_n^2\xi} + \theta_p \tag{13b}$$

where $\theta_p$ the particular integral of Eq. (11), given as

$$\theta_p = \frac{G_2'}{12}(1-\eta^4) + \frac{G_1}{2}(1-\eta^2) \tag{14}$$

where $G_2' = 4\Omega^2 G_2$. The functions $f_n$ and $g_n$ satisfy the following differential equations:

$$\frac{\partial^2 f_n}{\partial\eta^2} + \lambda^2\left(\frac{\lambda^2}{Pe^2} - u(\eta)\right)f_n = 0 \tag{15}$$

$$\frac{\partial^2 g_n}{\partial\eta^2} + \beta^2\left(\frac{\beta^2}{Pe^2} + u(\eta)\right)g_n = 0 \tag{16}$$

Solving Eqs. (15) and (16), the following functional forms can be obtained for $f_n$ and $g_n$:

$$f_n = e^{-\frac{1}{2}i\eta^2\lambda_n\sqrt{\Omega}}\,{}_1F_1\left[-\frac{i(Pe^2\lambda_n - \lambda_n^3 + iPe^2\sqrt{\Omega} + Pe^2\lambda_n\Omega)}{4Pe^2\sqrt{\Omega}};\ \frac{1}{2};\ i\eta^2\lambda_n\sqrt{\Omega}\right] \tag{17a}$$

$$g_n = \mathrm{e}^{-\frac{1}{2}\eta^2\beta_n\sqrt{\Omega}}\,{}_1F_1\left[-\frac{Pe^2\beta_n+\beta_n^3-Pe^2\sqrt{\Omega}+Pe^2\beta_n\Omega}{4Pe^2\sqrt{\Omega}};\ \frac{1}{2};\eta^2\beta_n\sqrt{\Omega}\right] \tag{17b}$$

where ${}_1F_1(M;N;Z)=\sum_{k=0}^{\infty}\frac{M_k}{N_k}\frac{Z^k}{k!}$. The functions $f_n$ and $g_n$ satisfy the following boundary conditions:

$$f_n'(0)=0,\quad f_n(1)=0,\quad g_n'(0)=0,\quad g_n(1)=0 \tag{18}$$

These boundary conditions can be used to obtain the eigenvalues and, the coefficients in the following closed forms (for details, see Appendix A):

$$A_n=\frac{\int_0^1\left[\frac{\lambda_n^2}{Pe^2}-u(\eta)\right]f_n\,\mathrm{d}\eta}{\int_0^1\left[\frac{2\lambda_n^2}{Pe^2}-u(\eta)\right]f_n^2\,\mathrm{d}\eta}=\frac{2}{\left(\lambda_n\frac{\partial f_n(1)}{\partial\lambda}\right)_{\lambda=\lambda_n}} \tag{19}$$

$$B_n=\frac{\int_0^1\left[\frac{\beta_n^2}{Pe^2}+u(\eta)\right]g_n\,\mathrm{d}\eta}{\int_0^1\left[\frac{2\beta_n^2}{Pe^2}+u(\eta)\right]g_n^2\,\mathrm{d}\eta}=-\frac{2}{\left(\beta_n\frac{\partial g_n(1)}{\partial\beta}\right)_{\beta=\beta_n}} \tag{20}$$

The dimensionless mean temperature can be obtained as

$$\theta_{m,i}(\xi)=\frac{\int_0^1 u(\eta)\theta_i\,\mathrm{d}\eta}{\int_0^1 u(\eta)\,\mathrm{d}\eta} \tag{21}$$

The Nusselt number can finally be obtained as $Nu_i=-\frac{4\frac{\partial\theta_i}{\partial\eta}_{\eta=1}}{\theta_{m,i}}$, which leads to the following final expression:

$$Nu(\xi)=\frac{\left(4\sum_{n=1}^{\infty}B_n\mathrm{e}^{-\beta_n^2\xi}g_n'(1)-\frac{G_2'}{3}-G_1\right)\int_0^1 u(\eta)\,\mathrm{d}\eta}{\sum_{n=1}^{\infty}B_n\mathrm{e}^{-\beta_n^2\xi}\left(\frac{g_n'(1)}{\beta_n^2}+\frac{\beta_n^2}{Pe^2}\int_0^1 g_n(\eta)\,\mathrm{d}\eta\right)-\int_0^1 u(\eta)\left(\frac{G_2'}{12}(1-\eta^4)+\frac{G_1}{2}(1-\eta^2)\right)\mathrm{d}\eta} \tag{22}$$

## 3. Results and discussion

The various cases have been studied taking numerical values representative of a typical electroosmotic flow, i.e. $\sigma=4\times10^{-4}$ S/m, $E_x=150$ K V/m, $\mu=9\times10^{-4}$ N s/m$^2$, $a=50$ μm, $k=0.6$ W/m K, $\zeta=-100$ mV, $\varepsilon=80$. Illustrative case studies are first executed by considering the variations of the parameter $G_1$, keeping all other parameters as unaltered. The corresponding temperature profiles are depicted in Fig. 2a–c. Because of symmetry of temperature profiles with respect to the centre line, the temperature distribution in the upper half of the channel is only plotted. Fig. 2a depicts the variations in the non-dimensional temperature profiles, as a function of the non-dimensional axial position, corresponding to, with $G_2\sim10^{-7}$. In this case, the channel wall temperature corresponding to $\xi>0$, i.e. $T_w$, is less than that corresponding to $\xi<0$, i.e. $T_0$. Because of the positive heat source term, the non-dimensional temperature, $\theta$, remains always positive, so that the fluid is always at a higher temperature than the channel walls. As the flow progresses along the axial direction, the local fluid temperature and the heat flux decreases. This is because of a progressive thickening of the thermal boundary layer, so that the temperature gradient prevailing across the thermal boundary layer diminishes continuously. A thermally fully developed state is reached at $\xi\approx10$, beyond which the amount of heat rejected from the channel walls is balanced by the volumetric internal energy generation due to Joule heating. Fig. 2b depicts the normalized temperature distribution for the case in which both Joule heating and viscous heating effects can be neglected (i.e., $G_1\approx0, G_2\approx0$), while the other parameters being kept as unaltered. Although in reality the Joule heating is always associated with electroosmotic flow, this exercise is executed to compare the present results with the classical benchmark solutions for thermally developing yet hydrodynamically developed slug (uniform) flows. It is observed from Fig. 2b that the normalized temperature decreases along the channel, as one advances towards further downstream direction, qualitatively analogous to the manner observed in Fig. 2a. Without any volumetric heat generation, the heat transfer between the channel and the fluid takes place only over the thermally developing region (up to $\xi\approx10$). Since the fluid temperature is always greater than the wall temperature over the thermal entrance region, the wall heat flux remains positive, irrespective of a continuously decreasing temperature difference between the bulk flow and the wall as one proceeds further downstream. Fig. 2c depicts the evolution of the temperature field along the channel for, $G_2'\sim10^{-6}$. In such as case, the wall is found to be hotter than the fluid at $\xi=0$. However, the fluid temperature subsequently increases because of the volumetric heating and thermal conditions maintained at the walls, till it exceeds the wall temperature. Beyond this, the temperature rise is solely due to the volumetric heating effects. Because of such transitions in the physical behaviour, cases with $G_1<0$ are characterized by much shorter thermal entrance lengths, as compared to the cases with. It is also interesting to observe that for $G_1<0$, the normalized fluid temperature ($\theta$) and the wall heat flux decreases, but the dimensional fluid temperature ($T$) increases due to volumetric heating, as the fluid progresses along the channel. This can be attributed to the fact that close to $\xi=0^+$, the fluid temperature is less than the wall temperature, whereas for higher values of $\xi$ the fluid temperature is likely to become greater than the wall temperature, depending on the strength of volumetric heating. In between, the flow passes through a regime so that the difference in temperature between the wall and the fluid locally tends to zero, which occurs between $\xi=0.5$ and $\xi=1$, for the situation depicted in Fig. 2c. This, in practice,

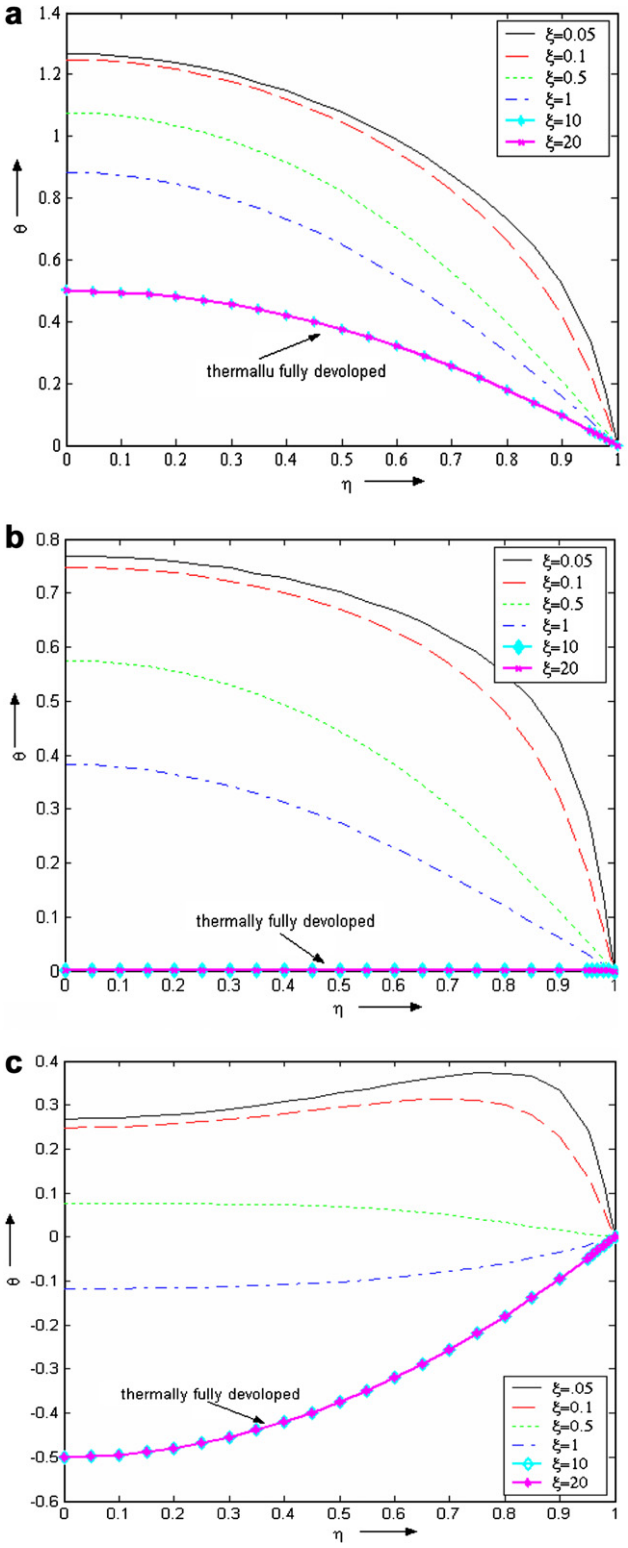


Fig. 2. Non-dimensional temperature distribution across the channel at different downstream locations at $Pe = 1$, $\Omega = 1$ for: (a) $G_1 = 1$, (b) $G_1 = 0$, (c) $G_1 = -1$.

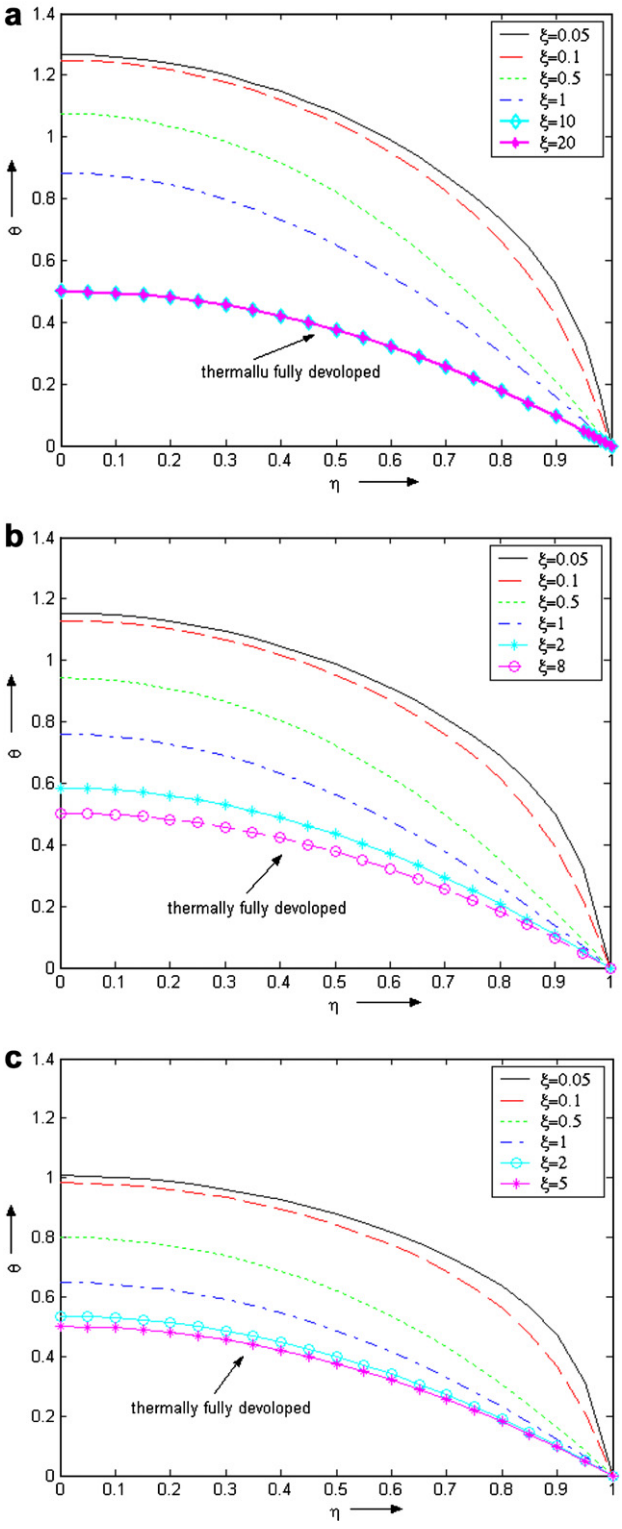


Fig. 3. Non-dimensional temperature distribution across the channel at different downstream locations at $Pe = 1$, $G_1 = 1$ for: (a) $\Omega = 1$, (b) $\Omega = 0$, (c) $\Omega = -1$.

delays the attainment of the thermally fully developed state, which is characterized by an invariant $\frac{T-T_w}{T_b-T_w}$ along the channel axis, $T_b$ being the bulk mean temperature of flow.

Fig. 3 depicts the variations in the temperature profile with changes in values of the parameter $\Omega$, with $Pe = 1$, $G_1 = 1$, and $G_2 \sim 10^{-7}$. Although the qualitative trends in

the temperature profiles are observed to be somewhat similar for the three different values of $\Omega$ being considered ($-1$, 0, and 1), the corresponding thermal entrance lengths are found to be markedly different. With a favorable axial pressure gradient (signified by positive values of $\Omega$), a stronger axial velocity component delays the growth of the thermal boundary layer, for a given Prandtl number. Thus, for $\Omega = 1$, the thermal entrance length is observed to be the greatest ($\xi = 10$), whereas the same appears to be progressively lower for $\Omega = 0$ and $\Omega = -1$, for which the values of $\xi$ are approximately 8 and 5, respectively.

It is important to mention here that the parameters assumed for obtaining the plots in Figs. 2 and 3 conform to the cases in which the viscous heating effects are negligible in comparison to the Joule heating effects ($G_2/G_1 \approx 10^{-6}$). However, in order to assess the influences of viscous dissipation, one needs to consider higher values of $\Omega$, so that the term $G_2'(G_2' = 4\Omega^2 G_2)$ becomes significant as compared to the Joule heating term, $G_1$. The distinctive influences of the parameter $\Omega$, reminiscent of these conditions, are captured through the plots depicted in Fig. 4a–c, which demonstrate the temperature distributions for

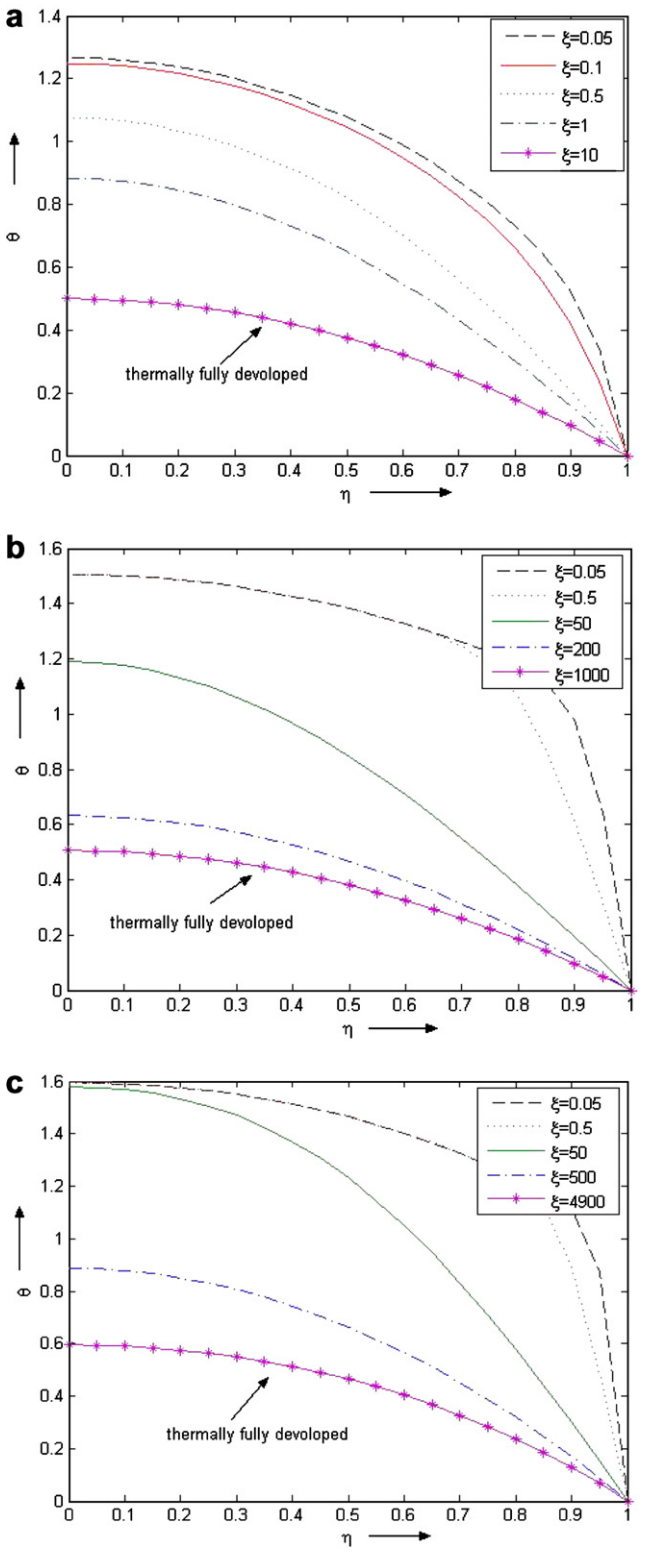


Fig. 4. Non-dimensional temperature distribution across the channel at different downstream locations for $Pe = 1$, $G_1 = 1$, with: (a) $G_2' = 1.14\times 10^{-6}$, (b) $G_2' = 0.07128$, (c) $G_2' = 1.14048$.

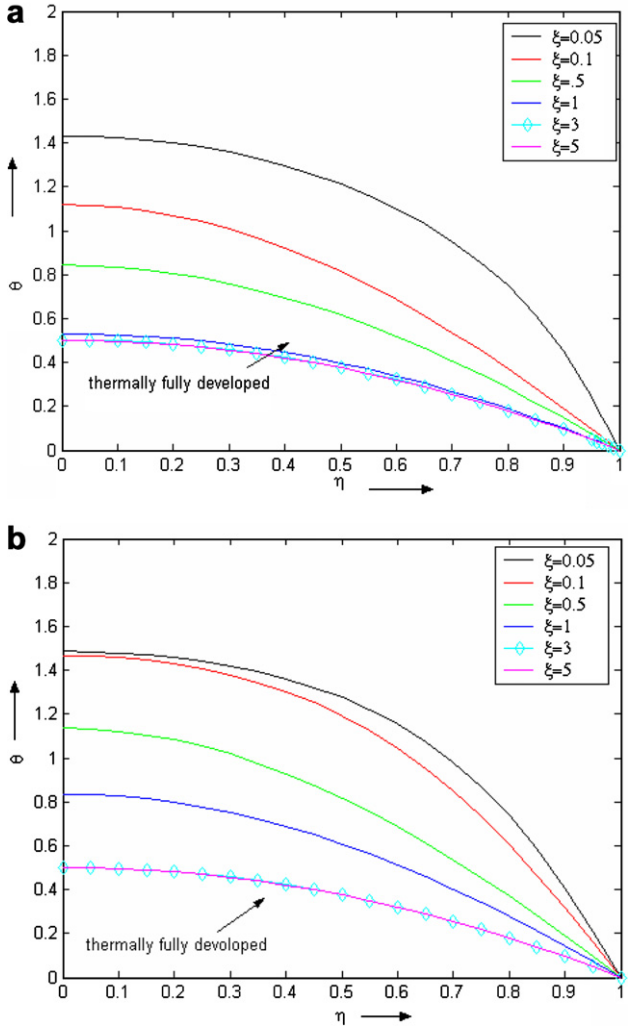


Fig. 5. Non-dimensional temperature distribution across the channel at different downstream locations for $G_1 = 1$, $G_2' \approx 0$: (a) $Pe = 2.5$ and (b) $Pe = 5$.

three different orders of magnitude of $\Omega$, with $Pe = 1$, and $G_1 = 1$. Fig. 4a corresponds to $\Omega = 0$, for which the value of $G_2'$ turns out to be 0. The flow becomes thermally fully developed at about $\xi = 10$. Fig. 4b corresponds to $\Omega = 250$, for which $G_2' = 0.07128$. It can be observed that such a high value of $\Omega$ results in large axial velocity scales, and hence the thermal boundary layer develops over a much larger distance ($\xi = 1000$) as compared to the previous case. Fig. 4c corresponds to $\Omega = 1000$, resulting in $G_2' = 1.14048$, which is of comparable order with the Joule heating term, $G_1 = 1$. In this case, the attainment of a thermally fully developed state is substantially delayed, and occurs at approximately $\xi = 4900$. It can also be observed that the final temperature is appreciably higher for the case with $\Omega = 1000$, as compared to the cases with $\Omega = 250$ and $\Omega = 1$, attributed to the significant contribution of viscous dissipation effects in the former case.

In addition to temperature profile shown in Figs. 1 and 5a and b show temperature variation for similar parameters but with different Peclet numbers, i.e. 2.5 and 5, respectively.The temperature profiles are very much similar in all respects because of similar heat generation and loss terms except for the fact that the thermally fully developed state is attained at smaller values of $\xi$ (non dimensional zed axial distance) for increasing Peclet numbers.

Fig. 6 depicts the variations in $Nu$ for different values of $\Omega$, with $Pe = 5$ and $G_1 = 1$. For lower values of $\Omega$, the quantitative differences in the values of $Nu$ with variations in $\Omega$ are not too prominent, except for the fact that the flow reaches a thermally fully developed state at somewhat larger axial distances for higher values of $\Omega$. However, for significantly large values of $\Omega$, the $Nu$ increases dramatically in the thermal entrance region, such as the case with $\Omega = 250$, as evident from Fig. 5. In such cases, the viscous dissipation becomes of comparable order with the Joule heating, for which the driving temperature gradients for

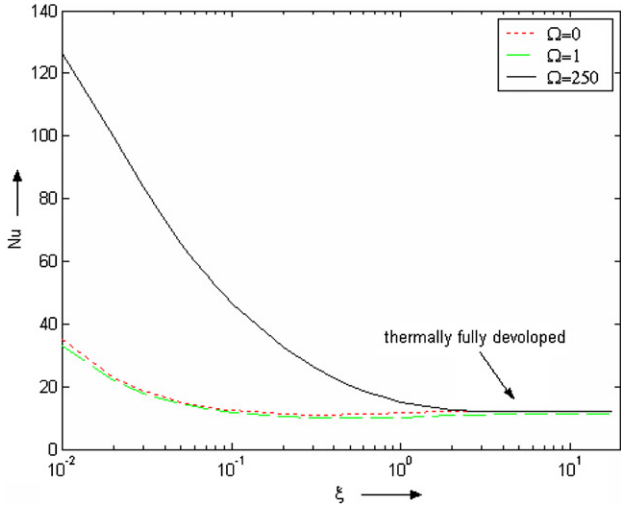


Fig. 6. Nusselt number for different values of $\Omega$, with $Pe = 5$, $G_1 = 1$, $G_2 = 7.128 \times 10^{-6}$.

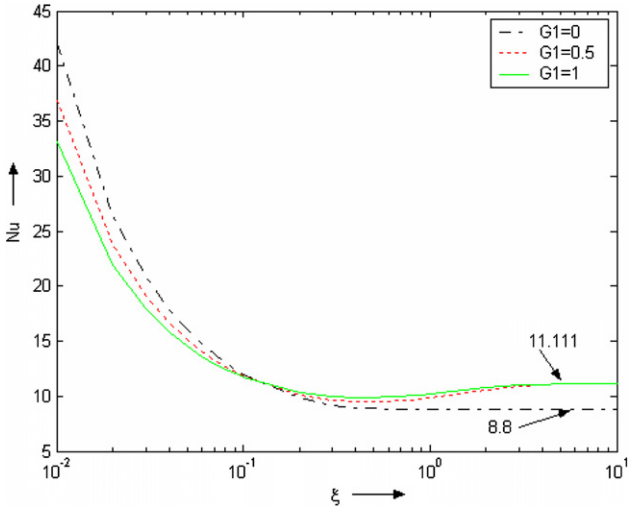


Fig. 7. Nusselt number variations for different values of $G_1$, with $Pe = 5$, $\Omega = 1$.

convective heat transfer are much more, for a given thermal boundary layer thickness. In reality, this effect is further aggravated by the fact that a higher value of $\Omega$ is also characterized with a thinner thermal boundary layer at a given axial location, which in turn magnifies the local temperature gradients prevailing across the thermal boundary layer even further. As a combined consequence of these two effects, the flow becomes thermally fully developed at about $\xi = 20$ for $\Omega = 250$, which is higher than the thermal entrance lengths obtained for the other two chosen values of $\Omega$ (for which $\xi = 8$, approximately).

Fig. 7 depicts the sensitivities of $Nu$ with varying $G_1$, for $Pe = 5$, and $\Omega = 1$. Although the value of $G_2$ would also change with different values of $G_1$, its effect is observed to be negligible for the ranges of values considered. It can be seen that the value of $Nu$ approaches the same asymptotic limit for different magnitudes of the heat source term, so long as $G_1 \neq 0$. For $G_1 = 0$, the value of $Nu$ depends on the first few terms of the expansion series representing the temperature distribution, and approaches a different limit. Particular interesting cases with classical importance can also be retrieved from the present generalized model. For example, with $G_1 = 0$ and $\Omega = 0$, an asymptotic Nusselt number of 2.467 can be obtained, which exactly agrees with the classical result [15] of thermally fully developed flow in a parallel plate channel with plug-type velocity profiles and being subjected to isothermal wall conditions. On an other extreme, $G_1 = 0$ and $\Omega \to \infty$ yields an asymptotic Nusselt number of 7.54, which corresponds to the limiting case of thermally fully developed pressure-driven flow in a parallel plate channel with isothermal walls [15].

## 4. Conclusions

A semi-analytical approach towards the solution of extended Graetz problem for combined pressure-driven and electroosmotic flows in microchannels with step

changes in wall temperature has been presented in this study. From the analysis of the results obtained from the present model, following important inferences can be drawn:

- For low values of $\Omega$, the viscous dissipation effects are negligible in comparison to the Joule heating effects, in terms of dictating the temperature profiles and the consequent heat transfer characteristics.
- For positive values of $G_1$, the temperature decreases along the axial direction till a condition is reached when the Joule heating equals the heat lost by the fluid to the walls. For negative values of $G_1$, on the other hand, the temperature initially increases along the axial direction because of the combined effect of Joule heating and heat transfer from the wall. The temperature increases to a point where it becomes greater than the wall temperature and sets the heat transfer to the wall in equilibrium with Joule heating.
- Positive values of $\Omega$ (favorable pressure gradients) lead to enhanced axial velocity scales and necessitate larger axial distances to achieve a thermally fully developed state, whereas for negative values of $\Omega$ (adverse pressure gradients) the attainment of thermally fully developed state is substantially delayed.
- Substantially large positive values of $\Omega$ may render the viscous dissipation of comparable order as the Joule heating, which, aided by a thinning of the thermal boundary layer for higher axial velocities due to stronger favorable pressure gradients, might give rise to substantially higher rates of heat transfer in the thermal entrance region. However, for chosen sets of the parameters $G_1$ and $\Omega$, the Nusselt number in the thermally fully developed state virtually approaches similar asymptotic limits, except for the case with $G_1 = 0$ for which classical heat transfer results can be retrieved.

## Appendix A. Determination of the eigenvalues

As explained in the paper by Lahjomri and Ouabarra [16] the functions $f$ and $g$ satisfy the following differential equations:

$$\frac{\partial^2 f_n}{\partial \eta^2} + \lambda^2 \left( \frac{\lambda^2}{Pe^2} - u(\eta) \right) f_n = 0 \tag{A1}$$

$$\frac{\partial^2 g_n}{\partial \eta^2} + \beta^2 \left( \frac{\beta^2}{Pe^2} + u(\eta) \right) g_n = 0 \tag{A2}$$

coupled with the following boundary conditions

$$f'(0) = 0, \quad f(1) = 0, \quad g'(0) = 0, g(1) = 0 \tag{A3}$$

The fundamental problem associated with this system of equations is the determination of eigenvalues $\alpha_n$ and $\beta_n$ and the coefficients $A_n$ and $B_n$. We have the general solution for temperature distribution as follows:

$$\theta_1 = 1 + \sum_{n=1}^{\infty} A_n f_n(\eta) e^{\lambda_n^2 \xi} + \theta_p \tag{A4}$$

$$\theta_2 = \sum_{n=1}^{\infty} B_n g_n(\eta) e^{-\beta_n^2 \xi} + \theta_p \tag{A5}$$

From the considerations of the continuity of temperature and temperature gradient at $\xi = 0$, one may write

$$\theta_1 = \theta_2 \text{ at } \xi = 0 \ \forall \ 0 \leqslant \eta \leqslant 1 \tag{A6}$$

$$\frac{\partial \theta_1}{\partial \xi} = \frac{\partial \theta_2}{\partial \xi} \text{ at } \xi = 0 \ \forall \ 0 \leqslant \eta \leqslant 1 \tag{A7}$$

Substituting the solutions (A4) and (A5) in Eqs. (A6) and (A7), one may obtain the following equations with unknowns $A_n$ and $B_n$:

$$1 + \sum_{n=1}^{\infty} A_n f_n(\eta) = \sum_{n=1}^{\infty} B_n g_n(\eta) \tag{A8}$$

$$\sum_{n=1}^{\infty} \lambda_n^2 A_n f_n(\eta) = -\sum_{n=1}^{\infty} \beta_n^2 B_n g_n(\eta) \tag{A9}$$

Multiplying Eq. (A8) by $\left[\frac{\beta_m^2}{Pe^2} + u(\eta)\right] g_m$ and integrating the same with respect to $\eta$ from 0 to 1, one may obtain

$$\begin{aligned} \int_0^1 \left[ \frac{\beta_m^2}{Pe^2} + u(\eta) \right] g_m \, d\eta = B_m \int_0^1 \left[ \frac{\beta_m^2}{Pe^2} + u(\eta) \right] g_m^2 \, d\eta \\ + \sum_{n=1}^{\infty} A_n \int_0^1 \left[ -\frac{\beta_m^2}{Pe^2} - u(\eta) \right] g_m f_n \, d\eta \\ + \sum_{\substack{n=1 \\ (n \neq m)}}^{\infty} B_n \int_0^1 \left[ \frac{\beta_m^2}{Pe^2} + u(\eta) \right] g_m g_n \, d\eta \end{aligned} \tag{A10}$$

Eq. (A10) is obtained by utilizing the fact that function $g$ satisfies the following properties:

$$\int_0^1 \left[ \frac{\beta_m^2 + \beta_n^2}{Pe^2} + u(\eta) \right] g_m g_n \, d\eta = 0, \quad \beta_m \neq \beta_n \tag{A11}$$

$$\int_0^1 \left[ \frac{\beta_m^2 + \beta_n^2}{Pe^2} + u(\eta) \right] g_m g_n \, d\eta \neq 0, \quad \beta_m = \beta_n \tag{A12}$$

Using the boundary conditions given by Eq. (A3), Eq. (10) yields

$$\begin{aligned} \int_0^1 \left[ \frac{\beta_m^2}{Pe^2} + u(\eta) \right] g_m \, d\eta = B_m \int_0^1 \left[ \frac{\beta_m^2}{Pe^2} + u(\eta) \right] g_m^2 \, d\eta \\ + \sum_{n=1}^{\infty} A_n \int_0^1 \left[ -\frac{\beta_m^2}{Pe^2} - u(\eta) \right] g_m f_n \, d\eta \\ - \sum_{\substack{n=1 \\ (n \neq m)}}^{\infty} B_n \frac{\beta_n^2}{Pe^2} \int_0^1 g_m g_n \, d\eta \end{aligned} \tag{A13}$$

Similarly, multiplying the Eq. (A9) by $\frac{g_m}{Pe^2}$ and integrating with respect to $\eta$ from 0 to 1, one gets

$$-\sum_{n=1}^{\infty} B_n \frac{\beta_n^2}{Pe^2} \int_0^1 g_m g_n \, d\eta = \sum_{n=1}^{\infty} A_n \frac{\lambda_n^2}{Pe^2} \int_0^1 g_m f_n \, d\eta \tag{A14}$$

After some manipulation, Eq. (A13) takes the following form, by utilizing Eq. (A14)

$$\int_0^1 \left[\frac{\beta_m^2}{Pe^2}+u(\eta)\right] g_m \,\mathrm{d}\eta = B_m \int_0^1 \left[\frac{2\beta_m^2}{Pe^2}+u(\eta)\right] g_m^2 \,\mathrm{d}\eta + \sum_{n=1}^{\infty} A_n F_{n,m} \tag{A15}$$

where

$$F_{n,m} = \int_0^1 \left[\frac{\lambda_n^2-\beta_m^2}{Pe^2}-u(\eta)\right] g_m f_n \,\mathrm{d}\eta \tag{A16}$$

Again, multiplying Eq. (A8) by $\left[\frac{\lambda_m^2}{Pe^2}-u(\eta)\right] f_m$, and utilizing similar properties as given by Eqs. (A11) and (A12) for $f_n$, one may obtain the following expression:

$$\int_0^1 \left[\frac{\lambda_m^2}{Pe^2}-u(\eta)\right] f_m \,\mathrm{d}\eta = -A_m \int_0^1 \left[\frac{2\lambda_m^2}{Pe^2}-u(\eta)\right] f_m^2 \,\mathrm{d}\eta + \sum_{n=1}^{\infty} B_n F_{m,n} \tag{A17}$$

It can be shown that the functions $F_{n,m}$ and $F_{m,n}$ are zero, corresponding to any legitimate value of $m$ and $n$. If one considers any two solutions $f_n$ and $g_m$ of Eqs. (A1) and (A2), multiplies the first one by $g_m$ and the second one by $f_n$, the following equations can readily be obtained:

$$g_m(1) f_n'(1) - f_n(1) g_m'(1) + (\lambda_n^2+\beta_m^2) F_{n,m} = 0 \tag{A18}$$

$$g_n(1) f_m'(1) - f_m(1) g_n'(1) + (\lambda_m^2+\beta_n^2) F_{m,n} = 0 \tag{A19}$$

Using the boundary conditions given by Eq. (A3), it is trivial to verify that $F_{n,m}$ and $F_{m,n}$ are zero for any permissible value of $m$ and $n$. Using Eqs. (A15), (A17), (A18) and (A19), one may get the expressions for $A_n$ and $B_n$, as follows:

$$A_n = \frac{\int_0^1 \left[\frac{\lambda_n^2}{Pe^2}-u(\eta)\right] f_n \,\mathrm{d}\eta}{\int_0^1 \left[\frac{2\lambda_n^2}{Pe^2}-u(\eta)\right] f_n^2 \,\mathrm{d}\eta} = \frac{2}{\left(\lambda_n \frac{\partial f_n(1)}{\partial \lambda}\right)_{\lambda=\lambda_n}} \tag{A20}$$

$$B_n = \frac{\int_0^1 \left[\frac{\beta_n^2}{Pe^2}+u(\eta)\right] g_n \,\mathrm{d}\eta}{\int_0^1 \left[\frac{2\beta_n^2}{Pe^2}+u(\eta)\right] g_n^2 \,\mathrm{d}\eta} = -\frac{2}{\left(\beta_n \frac{\partial g_n(1)}{\partial \beta}\right)_{\beta=\beta_n}} \tag{A21}$$

## References


[1] S. Das, S. Chakraborty, Analytical solutions for velocity, temperature and concentration distribution in electroosmotic microchannel flows of a non-Newtonian bio-fluid, Anal. Chim. Acta 559 (2006) 15–24.

[2] S. Das, T. Das, S. Chakraborty, Modeling of coupled momentum, heat and solute transport during DNA hybridization in a microchannel in presence of electro-osmotic effects and axial pressure gradients, Microfluidics Nanofluidics 2 (2006) 37–49.

[3] S. Das, T. Das, S. Chakraborty, Analytical solutions for rate of DNA hybridization in a microchannel in presence of pressure-driven and electroosmotic flows, Sensors Actuators B 114 (2006) 957–963.

[4] S. Das, S. Chakraborty, Transverse electrodes for improved DNA hybridization in microchannels, AIChE J. 53 (2007) 1086–1099.

[5] D. Maynes, B.W. Webb, Fully-developed thermal transport in combined pressure and electroosmotically driven flow in microchannels, J. Heat Transfer 125 (2003) 889–895.

[6] S. Chakraborty, Analytical solutions of Nusselt number for thermally fully developed flow in microtubes under a combined action of electroosmotic forces and imposed pressure gradients, Int. J. Heat Mass Transfer 49 (2006) 810–813.

[7] K. Horiuchi, P. Dutta, Joule heating effects in electroosmotically driven microchannel flows, Int. J. Heat Mass Transfer 47 (2004) 3085–3095.

[8] L. Graetz, Uber die Warmeleitungsfahighevon von Flussingkeiten, Part 1, Ann. Phys. Chem. 18 (1883) 79–94.

[9] J.R. Sellars, M. Tribus, J.S. Klein, Heat transfer to laminar flow in a round tube or flat conduit—the Graetz problem extended, Trans. ASME 78 (1956) 441–448.

[10] J. Lahjomri, A. Oubarra, Analytical solution of the Graetz problem with axial conduction, ASME J. Heat Transfer 121 (1999) 1078–1083.

[11] R.J. Hunter, Zeta Potential in Colloid Science: Principles and Application, Academic Press, London, New York, 1981.

[12] T.A. Ameel, X. Wang, R.F. Barron, R.O. Warrington, Laminar forced convection in a circular tube with constant heat flux and slip flow, Microscale Thermophys. Eng. 1 (1997) 303–320.

[13] P. Dutta, K. Horiuchi, H.-M. Yin, Thermal characteristics of mixed electroosmotic and pressure-driven microflows, Comput. Math. Appl. 52 (2006) 651–670.

[14] A. Barletta, E. Magyari, The Graetz–Brinkman problem in a plane-parallel channel with adiabatic-to-isothermal entrance, Int. Commun. Heat Mass Transfer 33 (2006) 677–685.

[15] L.C. Burmister, Convective Heat Transfer, Wiley, New York, 1994.

[16] J. Lahjomri, A. Oubarra, A. Alemany, Heat transfer by laminar Hartmann flow in thermal entrance region with a step change in wall temperature: the Graetz problem extended, Int. J. Heat Mass Transfer 45 (2002) 1127–1148.